ACS APPLIED MATERIALS & INTERFACES

Research Article

www.acsami.org

Side Chain Influence on the Morphology and Photovoltaic Performance of 5-Fluoro-6-alkyloxybenzothiadiazole and Benzodithiophene Based Conjugated Polymers

Guangwu Li,[†] Baofeng Zhao,[‡] Chong Kang,[†] Zhen Lu,[†] Cuihong Li,[†] Huanli Dong,[§] Wenping Hu,[§] Hongbin Wu,*[,‡] and Zhishan Bo*[,†]

[†]Beijing Key Laboratory of Energy Conversion and Storage Materials, College of Chemistry, Beijing Normal University, Beijing 100875, China

[‡]State Key Laboratory of Luminescent Materials and Devices, Institute of Polymer Optoelectronic Materials and Devices, South China University of Technology, Guangzhou 510640, China

[§]Beijing National Laboratory for Molecular Sciences, Key Laboratory of Organic Solids, Institute of Chemistry, Chinese Academy of Sciences, Beijing, 100190, China

Supporting Information

ABSTRACT: Three conjugated polymers (**P1**−**P3**) with benzodithiophene derivatives as the donor unit, 5-fluoro-6-(2-hexyldecyloxy)-4,7-di(thiophen-2-yl)benzo[c][1,2,5] thiadiazole as the acceptor unit and thiophene as the spacer were designed, synthesized, and used as donor materials for polymer solar cells (PSCs). The influence of side chains at the benzodithiophene unit on the performance of PSCs was investigated. PSCs with the blend of **P2**:$PC_{71}BM$ (1:2, by weight) as the active layer show the highest power conversion efficiency (PCE) of 6.88%, with an open circuit voltage (V_{oc}) of 0.76 V, a short circuit current (J_{sc}) of 14.67 mA/cm^2, and a fill factor (*FF*) of 0.62. Our research revealed that the variation of side chains had a great influence on the morphology of blend films, which is crucial to the performance of PSCs. As indicated by transmission electron microscopy, the blends of **P1**:$PC_{71}BM$ (1:2) and **P2**:$PC_{71}BM$ (1:2) formed nanofibers, whereas the blends of **P3**:$PC_{71}BM$ (1:2) formed spherical domains. Therefore, we concluded that formation of a more interpenetrating phase-separated donor−acceptor network with a larger interfacial area and proper percolation in the blends from **P1** to **P2** is mainly responsible for better performance in the corresponding devices.

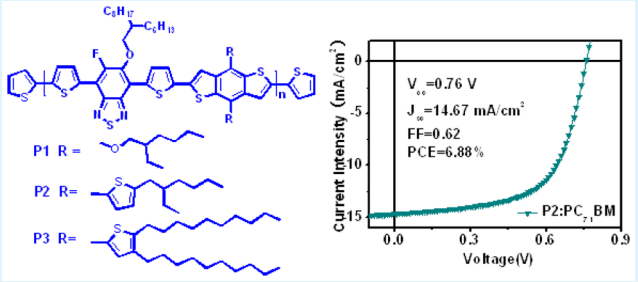

KEYWORDS: *5-fluoro-6-alkyloxybenzothiadiazole, benzodithiophene, polymer solar cells, mobility*

INTRODUCTION

Because of the characteristics such as being lightweight, flexible, and low-cost roll-to-roll processable, polymer solar cells (PSCs) have attracted intense research interest and their material catalogs and the performances have experienced a rapid development in the past few years.[1−4] The power conversion efficiency has been improved to 11%[5] through material design,[6−12] device structure innovation,[13−17] and interfacial engineering.[18−21] Thanks to a large interfacial area between the donor−acceptor (D−A) interface and the phase-separated interpenetrating network, the bulk heterojunction structure has been proven to be the most efficient structure to harvest photogenerated charge carriers in polymer solar cells.[22] Besides the rapid progress in the design and synthesis of nonfullerene or fullerene derivatives as electron acceptor materials,[23−29] the development of novel donor materials have also made a great deal of contribution to the efficiency improvement of PSCs. Especially, the donor−acceptor (D−A) alternating design strategy in the main chain, which takes advantage of the intramolecular charge transfer (CT) and can easily tune the band gap and energy level of conjugated polymers, has been proven to be a very useful approach to design new polymer donor materials. On the basis of this concept, a large number of new donor and acceptor building blocks have been successfully developed for the construction of new conjugated polymer donor materials for PSCs.[30−40]

Among a variety of building blocks for high-efficiency conjugated polymer donor materials, benzodithiophene and benzothiadiazole derivatives are promising donor and acceptor units, respectively. As a result, a large number of conjugated polymers with benzodithiophene as the donor unit and benzothiadiazole as the acceptor unit have been synthesized and used as the donor material for PSCs and high power conversion efficiency (PCE) up to 8% has been achieved.[41−51]

Received: January 4, 2015
Accepted: April 30, 2015
Published: April 30, 2015

DOI: 10.1021/acsami.5b00026
ACS Appl. Mater. Interfaces 2015, 7, 10710−10717

As a member of the benzothiadiazole family, 5-fluoro-6-alkyloxybenzothiadiazole has been demonstrated to be a useful acceptor unit in constructing high-efficiency D−A conjugated polymers.[52] In this article, from the view of design of new polymers to achieve high-performance PSCs, three polymers with 5-fluoro-6-(2-hexyldecyloxy)-4,7-di(thiophen-2-yl)benzo-[c][1,2,5]thiadiazole as the acceptor unit and benzodithiophene derivatives as the donor unit have been designed, synthesized, and used as donor materials for PSCs. It was found that the introduction of a fluorine atom on the benzothiadiazole unit can effectively lower the highest occupied molecular orbital (HOMO) and the lowest unoccupied molecular orbital (LUMO) energy level of the resulted conjugated polymers, while the introduction of a flexible alkoxy chain can increase the solubility of polymers. In comparison with alkoxy substitution, the introduction of thiophene side groups in the 4,8-positions of benzodithiophene unit can lower the HOMO level as well as increase the hole mobility of polymers. Deeper HOMO level is favored to afford higher V_{oc}, whereas higher hole mobility is usually furnished with higher J_{sc} and FF.[53−56] In this article, PSCs with the blend of **P2**:$PC_{71}BM$ (1:2, by weight) as the active layer exhibit a PCE of 6.88%, with a V_{oc} of 0.76 V, a J_{sc} of 14.67 mA/cm^2, and an FF of 0.62. Influences of lateral substituents at the benzodithiophene unit on the morphology of blend films and the device performance were also investigated.

RESULTS AND DISCUSSION

Material Synthesis and Characterization. The syntheses of monomer **M4** and copolymers **P1**−**P3** are outlined in Scheme 1. 4,7-Dibromo-5,6-difluorobenzothiadiazole (**1**) was synthesized in two steps from commercially available 4,5-difluorobenzene-1,2-diamine according to literature procedures.[53] The treatment of compound **1** with 2-hexdecan-1-ol and potassium *tert*-butoxide in tetrahydrofuran (THF) at 60 °C afforded 5-fluoro-6-(2-hexyldecanoxy)benzothiadiazole (**2**) in a yield of 59%. Suzuki cross-coupling of **2** with 4,4,5,5-tetramethyl-2-(thiophen-2-yl)-1,3,2-dioxaborolane and followed by bromination of the cross-coupling product with N-bromosuccinimide (NBS) in a solvent of chloroform at room temperature afforded **M4** in a total yield of 68%. Stille couplings of **M4** with **M1**, **M2**, and **M3** were carried out with $Pd(PPh_3)_4$ as the catalyst precursor in a solvent mixture of toluene and *N*,*N*-dimethylformamide (DMF) at 100 °C to afford polymers **P1**, **P2**, and **P3** in yields of 80%, 79%, and 71%, respectively. The solubility of **P1** and **P2** is poorer than **P3**. **P3** can be readily dissolved in chlorobenzene (CB), 1,2-dichlorobenzene (DCB), and 1,2,4-trichlorobenzene (TCB) at room temperature, whereas **P1** and **P2** are almost insoluble in the above-mentioned solvents at room temperature. Nevertheless, **P1** and **P2** are soluble in CB, DCB, and TCB at elevated temperature. Molecular weights and molecular weight distributions were determined by gel permeation chromatography (GPC) using TCB as an eluent at 150 °C with narrowly distributed polystyrenes as calibration standards and the results are summarized in Table 1. **P1** showed a number-average molecular weight (M_n) of 95.2 kg/mol, a weight-average molecular weight (M_w) of 195.8 kg/mol, and a polydispersity index (PDI) of 2.06. **P2** showed a M_n of 57.8 kg/mol, a M_w of 123.8 kg/mol, and a PDI of 2.14. **P3** showed a M_n of 86.4 kg/mol, a M_w of 182.4 kg/mol, and a PDI of 2.11. Thermogravimetric analysis (TGA) showed that all the polymers are of good thermal stability with the 5%

Scheme 1. Synthetic Route of Copolymers P1, P2, and P3[a]

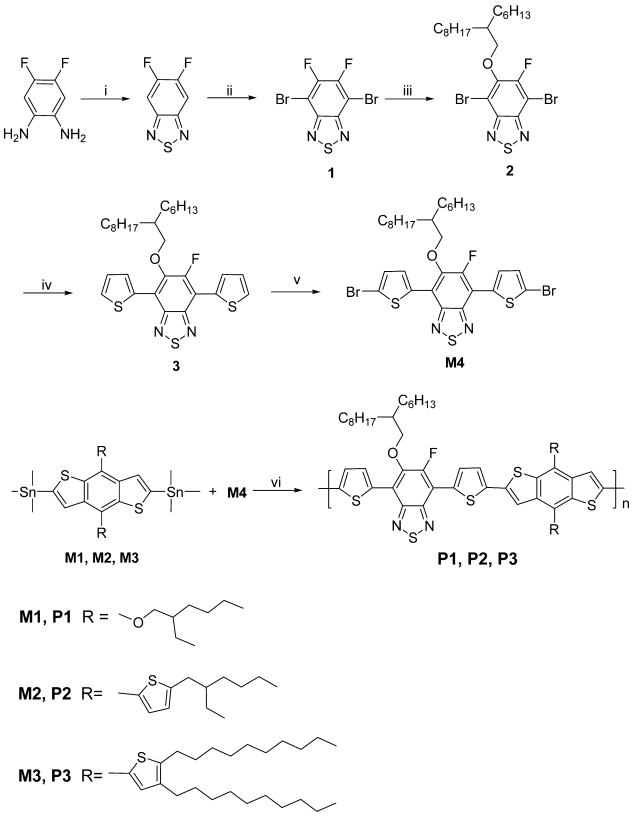

[a](i) Aniline, $SOCl_2$, toluene, 100 °C; (ii) NBS, H_2SO_4, 60 °C ; (iii) 2-hexyldecan-1-ol, $KOBu^t$, THF, 60 °C; (iv) $Pd_2(dba)_3$ (dba, dibenzylideneacetone), P(*o*-tol)$_3$, 4,4,5,5-tetramethyl-2-(thiophen-2-yl)-1,3,2-dioxaborolane, $NaHCO_3$, THF/H_2O, reflux; (v) NBS, $CHCl_3$, rt; (vi) $Pd(PPh_3)_4$, toluene/DMF (5:1, by volume), reflux.

Table 1. Molecular Weights and Thermal Properties of the Copolymers

polymer	M_n (kg/mol)[a]	M_w (kg/mol)[a]	PDI	T_d (°C)[b]
P1	95.2	195.8	2.06	325
P2	57.8	123.8	2.14	345
P3	86.4	182.4	2.11	345

[a]M_n, M_w, and PDI of polymers were determined by GPC at 150 °C using polystyrene standards with 1,2,4-trichlorobenzene as an eluent. [b]Decomposition temperatures were determined by TGA under N_2 based on 5% weight loss.

decomposition temperature up to 325 °C for **P1**, 345 °C for **P2**, and 345 °C for **P3** under a nitrogen atmosphere. No obvious glass transition was detected for all the three polymers via differential scanning calorimetry (DSC) measurements in the range of 20−300 °C. The packing of polymer chains in the solid state was investigated using powder X-ray diffraction (XRD) experiment. As shown in Figure 1, **P1** and **P2** exhibit two diffraction peaks in the powder XRD curves. The first peaks in a small-angle region, which reflexes the distance of polymer backbones separated by the flexible side chains, are located at 2θ of 4.78° for **P1** and 4.54° for **P2**, corresponding to distances of 18.50 and 19.44 Å, respectively. The second peak in the wide-angle region reflexes the $\pi-\pi$ stacking distances between polymer backbones, which are located at 2θ of 23.86° for P1 and 24.77° for **P2**, corresponding to distances of 3.73 and 3.59 Å, respectively. **P3** exhibits only a broad peak in the

DOI: 10.1021/acsami.5b00026
ACS Appl. Mater. Interfaces 2015, 7, 10710−10717

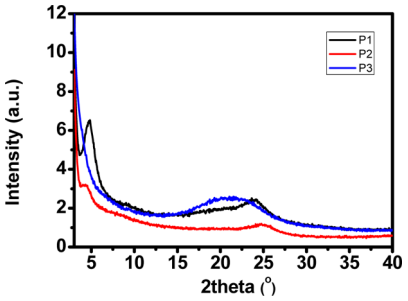

Figure 1. XRD patterns of powder polymer samples.

wide-angle region, which is located at 21.17°, corresponding to a distance of 4.18 Å. Compared with **P1** and **P2**, the larger $\pi-\pi$ stacking distance of **P3** in the solid state indicates that the two 4,5-didecylthiophienyl substituents at the 4,8-position of benzodithiophene unit can hamper the close and ordered packing of polymer chains in the solid state.

Optical Properties. The optical properties of **P1**−**P3** were investigated by UV−vis absorption spectroscopy and their absorption spectra in DCB solutions at room temperature, at 100 °C, and as thin films are shown in Figure 2, with the corresponding data summarized in Table 2. The films were spin-coated from polymer solutions in a concentration of 5 mg/mL and a spin rate of 1000 rpm. As shown in Figure 2, **P1**−**P3** exhibited similar film absorption spectra with two absorption bands in the visible region, which can be assigned to the $\pi-\pi^*$ transition of their main chain units and the CT absorption of polymer main chains. For **P1** and **P2** in DCB solutions, upon heating to 100 °C, the absorption maxima exhibited blue shifts of about 40 and 55 nm, respectively, while for **P3**, the blue shift is only about 7 nm. The above results indicated that **P1** and **P2** had a very strong tendency to aggregate at room temperature and the formed aggregation can be readily dissociated at elevated temperature. Since **P3** is soluble in DCB at room temperature, the blue shift of the absorption maximum is smaller. The film absorption onsets (λ_{onset}) of **P1**, **P2**, and **P3** are 698, 692, and 701 nm, respectively. The optical band gaps ($E_{g,opt}$) of **P1**, **P2**, and **P3** films were therefore calculated to be 1.78, 1.79, and 1.77 eV, respectively, according to the equation $E_{g,opt} = 1240/\lambda_{onset}$.

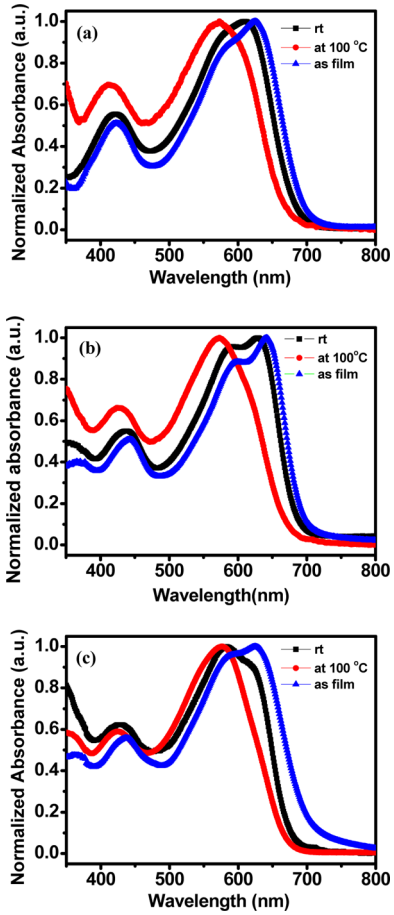

Figure 2. UV−vis absorption spectra of **P1** (a), **P2** (b), and **P3** (c) in DCB solutions at room temperature, at 100 °C, and as thin films.

Table 2. Optical and Electrochemical Properties of P1, P2, and P3

polymer	λ_{max} (nm)	λ_{edge} (nm)	$E_{g,opt}$ (eV)[a]	HOMO (eV)	LUMO (eV)[b]
P1	419, 624	698	1.78	−5.25	−3.47
P2	442, 641	692	1.79	−5.29	−3.50
P3	434, 624	701	1.77	−5.30	−3.53

[a]Calculated from the absorption band edge of the copolymer film, $E_{g,opt} = 1240/\lambda_{edge}$. [b]Calculated by the equation $E_{LUMO} = E_{HOMO} + E_{g,opt}$.

Electrochemical Properties. Electrochemical properties of **P1**, **P2**, and **P3** were investigated by cyclic voltammetry (CV) using a standard three-electrodes electrochemical cell. As shown in Figure 3, these three polymers exhibited quasi reversible redox processes. The onset oxidation potentials of polymer films for **P1**, **P2**, and **P3** are 0.54, 0.58, and 0.59 V, respectively. HOMO levels of **P1**, **P2**, and **P3** were determined, using the equation $E_{HOMO} = -e(E_{ox} + 4.71)$, to be −5.25, −5.29, and −5.30 eV, respectively. LUMO levels of **P1**, **P2**, and **P3** were therefore calculated according to the equation $E_{LUMO} = E_{HOMO} + E_{g,opt}$ to be −3.47, −3.50, and −3.53 eV, respectively. As expected, the replacing alkoxy side chain with alkylthienyl group slightly lowers the HOMO and LUMO level of polymers. The data are also summarized in Table 2.

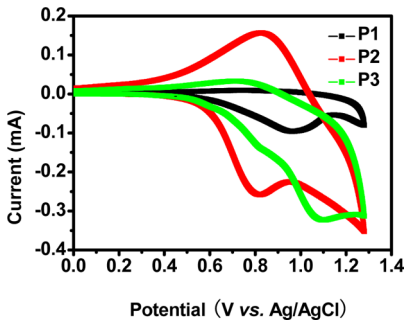

Figure 3. Cyclic voltammograms of **P1**, **P2**, and **P3** in films on a platinum electrode in 0.1 mol/L Bu_4NPF_6 acetonitrile solution at a scan rate of 100 mV/s.

Charge Transport Properties. As charge recombination is a significant loss mechanism for photocurrent and slow charge carrier determines the charge recombination process in polymer solar cells, it is important to maintain balanced charge carrier mobilities in a working device. Since electron mobility in the phenyl-C_{61}-butyric acid methyl ester ($PC_{71}BM$) domain can reach 10^{-2} cm^2 V^{-1} s^{-1}, it is desired to have hole mobility up to

DOI: 10.1021/acsami.5b00026
ACS Appl. Mater. Interfaces 2015, 7, 10710−10717

10^{-4}~10^{-3} cm^2 V^{-1} s^{-1} to avoid severe space charge buildup and the concomitant charge recombination. To investigate the charge transport properties of the resulted polymers, field-effect transistors (FETs) using the polymers as an active layer were fabricated, in which a top-contact configuration on Si/SiO_2 substrates was employed, with low-resistance Si as the gate and SiO_2 (300 nm) as the gate insulator, respectively. Polymer thin films were spin-coated on the octadecylsilane (OTS)-modified Si/SiO_2 substrates from DCB solutions, and Au electrodes with a thickness of 25 nm were thermally evaporated onto polymer thin films in vacuum. The transfer and output characteristic curves of FET devices are shown in Figure 4. Hole mobility (μ)

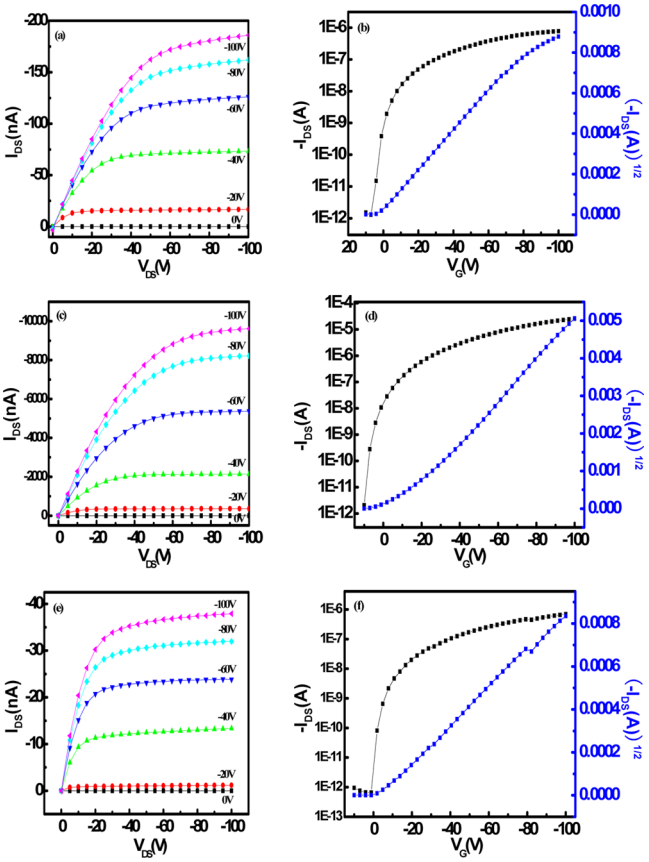

Figure 4. Transfer characteristics and output characteristics of the OFETs for **P1** (a, b), **P2** (c, d), and **P3** (e, f).

was deduced from the derivative plots in the saturated regime through the equation $I_{DS} = \mu(W/2L)C_i(V_G - V_T)^2$, where I_{DS} is the drain current, W is the channel width, L is the channel length, C_i is the capacitance per unit area of the gate dielectric layer (SiO_2, 300 nm, C_i = 11 nF/cm^2), and V_G and V_T are the gain voltage and threshold voltage, respectively. Hole mobilities of **P1**, **P2**, and **P3** are 2.44×10^{-3}, 9.03×10^{-2}, and 2.17×10^{-3} cm^2 V^{-1} s^{-1}, respectively, which are comparable with the electron mobility of $PC_{71}BM$. Besides the extracted hole mobilities, other parameters likes V_T and on/off ratios are also summarized in Table 3 for comparison, and the experimental details and more organic field-effect transistors (OFET) results are shown in Table 2 of the Supporting Information.

Photovoltaic Properties. To evaluate the photovoltaic performance of **P1**–**P3**, a series of polymer solar cells with device structure of indium tin oxide (ITO)/poly(3,4-ethylenedioxythiophene):poly(styrenesulfonate) (PEDOT:PSS)/active layer/LiF/Al were fabricated. After careful optimization of the weight ratio between polymer/$PC_{71}BM$, the concentration of blend solution, the thickness of the active layer, and film morphology via the use of additive like 1,8-diiodooctane, best device performance was reached and the J–V curves of the corresponding devices under simulated solar illumination (AM 1.5G, 100 mW cm^{-2}) are shown in Figure 5,

Table 3. FET Properties of the Pure Polymer Films

polymers	on/off	μ (cm^2/(V s))	V_T (V)
P1	6.18×10^5	2.44×10^{-3}	−2.3
P2	1.22×10^7	9.03×10^{-2}	−13.1
P3	1.06×10^6	2.17×10^{-3}	−5.3

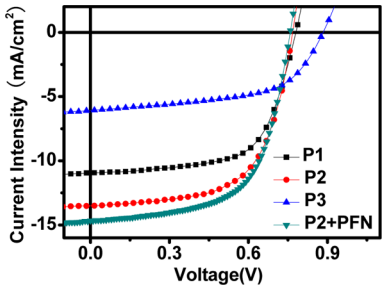

Figure 5. J–V characteristics of devices based on **P1**–**P3** under solar illumination (AM 1.5G, 100 mW/cm^2).

with the deduced parameters summarized in Table 4. With the device configuration of ITO/PEDOT:PSS/active layer/LiF/Al, the devices based on **P1**–**P3** showed PCE of 5.54%, 6.43%, and 3.07%, respectively. For all polymers, a D–A ratio of 1:2 gave the best results. Since the band gap and the electronic properties of the three polymers are very close to each other, the improved J_{sc} and better overall device performance in **P2** devices were mainly attributed to the observed higher space charge limited current (SCLC) mobility, which were measured by using the SCLC method and the results are summarized in Table 4. To further improve the performance of **P2**, inverted devices with a configuration of ITO/PFN/active layer/MoO_3/Al were fabricated[15] and a PCE of 6.88% was achieved, with a V_{oc} of 0.76 V, a J_{sc} of 14.67 mA/cm^2, and an *FF* of 0.62. The replacement of the alkyloxy side chain with the alkylthienyl side group has been demonstrated to be an effective strategy to enhance the performance of PSCs. In comparison with **P1**, **P2** carrying alkylthienyl side group gave much better photovoltaic performance, which is consistent with the results from the literature.[12,53,54] PSCs based on the double alkylthienyl substituted **P3** gave a high V_{oc} of 0.89 V, a lower J_{sc} of 6.08 mA/cm^2, and a PCE of 3.07%. The high V_{oc} for **P3**-based devices is probably due to two reasons: the first one is **P3** has the deepest HOMO level among these three polymers and the second one is that **P3** is an amorphous polymer (vide supra). The morphology of the active layer can influence the V_{oc} of devices. Many examples have shown that the formation of large spherical $PC_{71}BM$ aggregates usually give high V_{oc}, but poor PCE.[57,58] As confirmed by the XRD measurement, the crystallinity of **P3** is much poorer than that of **P2**. It has been demonstrated that increasing the crystallinity of polymers can shift the absorption onset in the dry films and decrease the open-circuit voltage.[58,59]

Figure 6a shows the UV–vis absorption spectra of blend films used as the active layer. All the blend films show a broad

DOI: 10.1021/acsami.5b00026
ACS Appl. Mater. Interfaces 2015, 7, 10710–10717

Table 4. Photovoltaic Performances and SCLC Mobilities of Polymer:$PC_{71}BM$ Blend Films

polymer	D−A ratio	J_{sc} (mA/cm^2)	V_{oc} (V)	*FF*	PCE (average)[c]	thickness (nm)	SCLC mobilities (cm^2/(V s))
P1[a]	1:2	11.03	0.79	0.64	5.54% (5.35%)	110	2.81×10^{-5}
P2[a]	1:2	13.50	0.78	0.61	6.43% (6.34%)	105	1.03×10^{-4}
P2[b]	1:2	14.67	0.76	0.62	6.88% (6.74%)	107	
P3[a]	1:2	6.08	0.89	0.57	3.07% (2.87%)	82	1.01×10^{-6}

[a]Device structure: ITO/PEDOT:PSS/polymer:$PC_{71}BM$/LiF/Al. [b]Device structure: ITO/PFN/polymer:$PC_{71}BM$/MoO_3/Al. [c]Ten devices were used to get the average value.

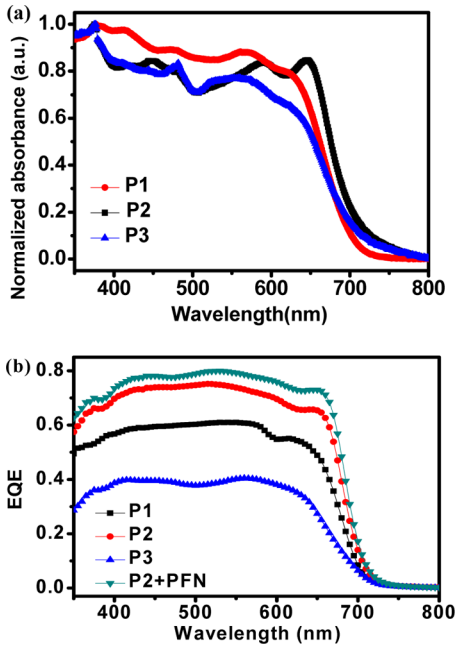

Figure 6. (a) UV−vis absorption spectra of blend films for polymers and $PC_{71}BM$; (b) EQE curves for the solar cells fabricated under the optimized conditions.

absorption ranging from 350 to 700 nm. **P2** exhibited two absorption peaks located at 591 and 646 nm, indicating that **P2** has good crystallinity in films. The result is consistent with the XRD result (vide supra). Figure 6b shows external quantum efficiencies (EQEs) or the incident photon-to-current efficiency (IPCE), the best **P1**−**P3** devices fabricated under the optimized condition, which are also used to verify the accuracy of the measured J_{sc} values in the *J*−*V* measurements. Consistent with the measured J_{sc} shown in Figure 4a and Table 4, **P2** showed a highest phototo-current response in the region of 350−700 nm and with an average EQE around 70%, while **P3** exhibited the lowest EQE. For the inverted device for **P2**, a maximal EQE around 80% was reached in the range of 450−550 nm, implying a very efficient photoconversion process and balanced charge transport in the devices. Furthermore, the calculated J_{sc} obtained by integrating the product of the EQE with the AM 1.5G solar spectrum agreed with the measured value to within 3%.

Film Morphology. To get further insight into the impact of molecular structure on the device performance, morphologies of the blend films were investigated by tapping-mode AFM (TM-AFM). It is commonly accepted that the ideal morphology for the active layer is an interpenetrating bicontinuous network in which large interfacial area and phase-separated domain size of 10−20 nm can facilitate exciton dissociation and charge transport.[57] As shown in Figure 7a, the **P1**:$PC_{71}BM$ blend films are homogeneous without apparent phase separation, with a root-mean-square (RMS) roughness of 1.75 nm. In contrast, the **P2**:$PC_{71}BM$ blend films as shown in Figure 7b exhibit obvious nanoscale phase separation and a RMS roughness of 1.53 nm. As for the **P3**:$PC_{71}BM$ (1:2) blend films, ellipsoidal cluster feature can be clearly observed as shown in Figure 7c, implying poor miscibility between **P3** and $PC_{71}BM$.

Since AFM images only provide the surface morphology information on blend films, we further apply transmission electron microscopy (TEM) to investigate the composition and in-depth morphology of the active layers. As shown in Figure 8, nanoscale phase-separated structure and curved fibrils were formed in the **P1**:$PC_{71}BM$ (1:2) blend films while more distinct and straight nanofibers features were clearly observed in the **P2**:$PC_{71}BM$ films. In contrast to the situation in **P1**/**P2**, much larger aggregates (with a diameter of 100−200 nm) were formed in the **P3**:$PC_{71}BM$ blend film, which is obviously preferable neither for efficient exciton dissociation nor for balanced charge transport. On the basis of the AFM and TEM results, we can conclude that the side chains of **P1**−**P3** have imparted great influence on the morphology of blend films in nanoscale as well as the performance of PSCs. The size of the side substituent can influence the solubility of polymers. **P3** with double alkyl substitution has the best solubility among

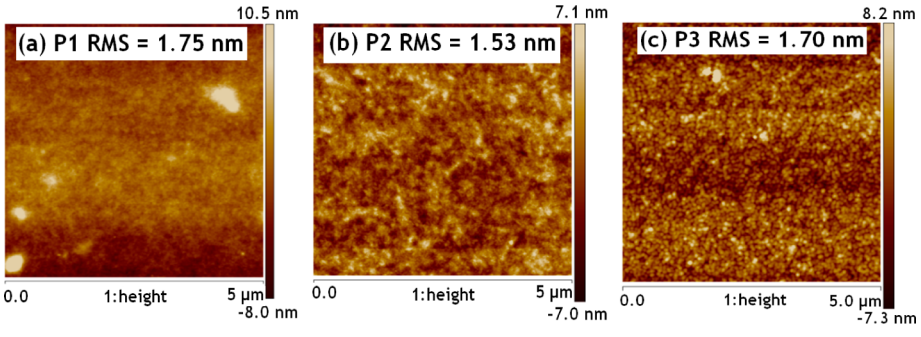

Figure 7. TM-AFM height images of polymer and $PC_{71}BM$ blend film (weight ratio 1:2): (a) **P1**:$PC_{71}BM$; (b) **P2**:$PC_{71}BM$; (c) **P3**:$PC_{71}BM$.

DOI: 10.1021/acsami.5b00026
ACS Appl. Mater. Interfaces 2015, 7, 10710−10717

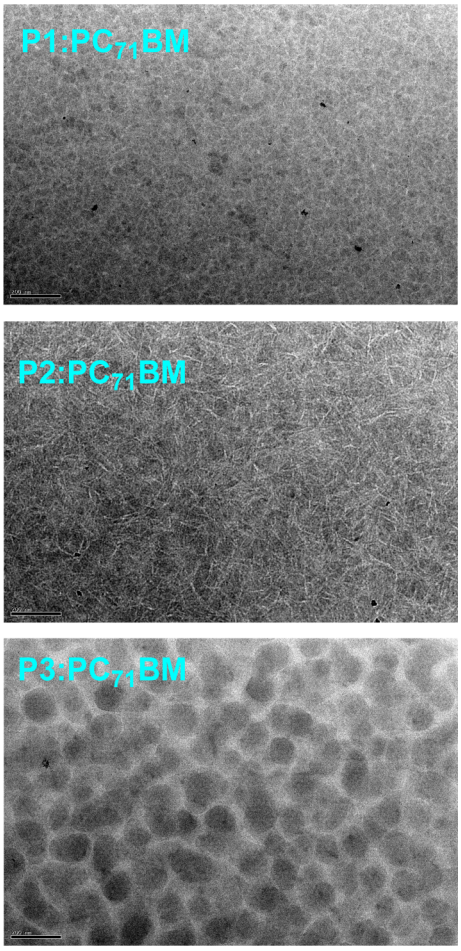

Figure 8. TEM images of polymer:$PC_{71}BM$ blend films in a weight ratio 1:2; the scale bar was 200 nm.

these three polymers. The solubility of **P2** is much poorer than **P3**. **P3** can be dissolved in chloroform at elevated temperature, whereas **P2** is insoluble in hot chloroform, but soluble in chlorobenzene at elevated temperature. Because of its poor solubility in DCB at room temperature, **P2** is prone to aggregate before the liquid−liquid phase separation occurs,[58] which can result in appropriate morphology and higher power conversion efficiency. Because of its good solubility in DCB, the liquid−liquid phase separation dominates in the **P3**:$PC_{71}BM$ system, which will result in large spherical $PC_{71}BM$ domains and lower power conversion efficiency.[58] More solvent choices are required to further eliminate the poor morphology of **P3** to achieve higher PCE.

CONCLUSION

Three conjugated polymers **P1**−**P3** based on 5-fluoro-6-alkyloxybenzothiadiazole as the acceptor unit, benzodithiophene derivatives as the donor unit, and thiophene as the spacer were designed, synthesized, and used as donor materials in PSCs. PSCs based on **P2**:$PC_{71}BM$ (1:2) gave the highest PCE of 6.88% with a J_{sc} of 14.67 mA/cm^2, a V_{oc} of 0.76 V, and an *FF* of 0.62. AFM and TEM investigations revealed that the side chains at the benzodithiophene unit have a great influence on the morphology of blend films. The **P1**:$PC_{71}BM$ and **P2**:$PC_{71}BM$ blend films are of interpenetrated fibrillar structures, which can facilitate the charge carrier transportation. The formation of spherical domains by $PC_{71}BM$ rich phase in the **P3**:$PC_{71}BM$ blend films hamper the charge transport in the active layer, which resulted in a smaller J_{sc} for **P3**:$PC_{71}BM$ based PSCs. The morphology difference is probably caused by the solubility difference of polymers. **P1** and **P2**, which have a poor solubility in the processing solvent, are prone to aggregate before the liquid−liquid phase separation occurs, resulting in appropriate morphology and higher power conversion efficiency. **P3** has good solubility in DCB; the liquid−liquid phase separation dominates during the film drying, resulting in large spherical $PC_{71}BM$ domains and lower power conversion efficiency.

ASSOCIATED CONTENT

Supporting Information

Synthesis and characterization of monomers and polymers; detailed results for OFET and PSCs. The Supporting Information is available free of charge on the ACS Publications website at DOI: 10.1021/acsami.5b00026.

AUTHOR INFORMATION

Corresponding Authors

*E-mail: hbwu@scut.edu.cn (H.W.).
*E-mail: zsbo@bnu.edu.cn (Z.B.).

Notes

The authors declare no competing financial interest.

ACKNOWLEDGMENTS

We express thanks for the financial support by the NSF of China (51003006 and 21161160443), the 973 Programs (2011CB935702), and the Fundamental Research Funds for the Central Universities.

REFERENCES

(1) Krebs, F. C. Processing and Preparation of Polymer and Organic Solar Cells. *Sol. Energy Mater. Sol. Cells* **2009**, *93*, 393−412.
(2) Günes, S.; Neugebauer, H.; Sariciftci, N. S. Conjugated Polymer-Based Organic Solar Cells. *Chem. Rev.* **2007**, *107*, 1324−1338.
(3) Dennler, G.; Scharber, M. C.; Brabec, C. J. Polymer-Fullerene Bulk-Heterojunction Solar Cells. *Adv. Mater.* **2009**, *21*, 1323−1338.
(4) Thompson, B. C.; Frechet, J. M. J. Organic photovoltaics - Polymer-Fullerene Composite Solar Cells. *Angew. Chem., Int. Ed.* **2008**, *47*, 58−77.
(5) Chen, C.-C.; Chang, W.-H.; Yoshimura, K.; Ohya, K.; You, J.; Gao, J.; Hong, Z.; Yang, Y. An Efficient Triple-Junction Polymer Solar Cell Having a Power Conversion Efficiency Exceeding 11%. *Adv. Mater.* **2014**, *26*, 5670−5677.
(6) Guo, X.; Facchetti, A.; Marks, T. J. Imide- and Amide-Functionalized Polymer Semiconductors. *Chem. Rev.* **2014**, *114*, 8943−9021.
(7) Chen, Y.; Wan, X.; Long, G. High Performance Photovoltaic Applications Using Solution-Processed Small Molecules. *Acc. Chem. Res.* **2013**, *46*, 2645−2655.
(8) Li, Y. Molecular Design of Photovoltaic Materials for Polymer Solar Cells: Toward Suitable Electronic Energy Levels and Broad Absorption. *Acc. Chem. Res.* **2012**, *45*, 723−733.
(9) Liang, Y.; Yu, L. A New Class of Semiconducting Polymers for Bulk Heterojunction Solar Cells with Exceptionally High Performance. *Acc. Chem. Res.* **2010**, *43*, 1227−1236.
(10) Coughlin, J. E.; Henson, Z. B.; Welch, G. C.; Bazan, G. C. Design and Synthesis of Molecular Donors for Solution-Processed High-Efficiency Organic Solar Cells. *Acc. Chem. Res.* **2013**, *47*, 257−270.
(11) Chen, J.; Cao, Y. Development of Novel Conjugated Donor Polymers for High-Efficiency Bulk-Heterojunction Photovoltaic Devices. *Acc. Chem. Res.* **2009**, *42*, 1709−1718.

DOI: 10.1021/acsami.5b00026
ACS Appl. Mater. Interfaces 2015, 7, 10710−10717

(12) Ye, L.; Zhang, S.; Huo, L.; Zhang, M.; Hou, J. Molecular Design toward Highly Efficient Photovoltaic Polymers Based on Two-Dimensional Conjugated Benzodithiophene. *Acc. Chem. Res.* **2014**, *47*, 1595−1603.
(13) Sun, Y.; Seo, J. H.; Takacs, C. J.; Seifter, J.; Heeger, A. J. Inverted Polymer Solar Cells Integrated with a Low-Temperature-Annealed Sol-Gel-Derived ZnO Film as an Electron Transport Layer. *Adv. Mater.* **2011**, *23*, 1679−1683.
(14) Li, W.; Furlan, A.; Hendriks, K. H.; Wienk, M. M.; Janssen, R. A. J. Efficient Tandem and Triple-Junction Polymer Solar Cells. *J. Am. Chem. Soc.* **2013**, *135*, 5529−5532.
(15) He, Z.; Zhong, C.; Su, S.; Xu, M.; Wu, H.; Cao, Y. Enhanced Power-Conversion Efficiency in Polymer Solar Cells Using an Inverted Device Structure. *Nat. Photonics* **2012**, *6*, 591−595.
(16) Gilot, J.; Wienk, M. M.; Janssen, R. A. J. Optimizing Polymer Tandem Solar Cells. *Adv. Mater.* **2010**, *22*, E67−E71.
(17) Kim, J. Y.; Lee, K.; Coates, N. E.; Moses, D.; Nguyen, T.-Q.; Dante, M.; Heeger, A. J. Efficient Tandem Polymer Solar Cells Fabricated by All-Solution Processing. *Science* **2007**, *317*, 222−225.
(18) He, Z.; Zhong, C.; Huang, X.; Wong, W.-Y.; Wu, H.; Chen, L.; Su, S.; Cao, Y. Simultaneous Enhancement of Open-Circuit Voltage, Short-Circuit Current Density, and Fill Factor in Polymer Solar Cells. *Adv. Mater.* **2011**, *23*, 4636−4643.
(19) Cheng, Y.-J.; Hsieh, C.-H.; He, Y.; Hsu, C.-S.; Li, Y. Combination of Indene-C60 Bis-Adduct and Cross-Linked Fullerene Interlayer Leading to Highly Efficient Inverted Polymer Solar Cells. *J. Am. Chem. Soc.* **2010**, *132*, 17381−17383.
(20) Mei, Q.; Li, C.; Gong, X.; Lu, H.; Jin, E.; Du, C.; Lu, Z.; Jiang, L.; Meng, X.; Wang, C.; Bo, Z. Enhancing the Performance of Polymer Photovoltaic Cells by Using an Alcohol Soluble Fullerene Derivative as the Interfacial Layer. *ACS Appl. Mater. Interfaces* **2013**, *5*, 8076−8080.
(21) Intemann, J. J.; Yao, K.; Li, Y.-X.; Yip, H.-L.; Xu, Y.-X.; Liang, P.-W.; Chueh, C.-C.; Ding, F.-Z.; Yang, X.; Li, X.; Chen, Y.; Jen, A. K. Y. Highly Efficient Inverted Organic Solar Cells Through Material and Interfacial Engineering of Indacenodithieno[3,2-b]thiophene-Based Polymers and Devices. *Adv. Funct. Mater.* **2014**, *24*, 1465−1473.
(22) Yu, G.; Gao, J.; Hummelen, J. C.; Wudl, F.; Heeger, A. J. Polymer Photovoltaic Cells: Enhanced Efficiencies via a Network of Internal Donor-Acceptor Heterojunctions. *Science* **1995**, *270*, 1789−1791.
(23) Earmme, T.; Hwang, Y.-J.; Murari, N. M.; Subramaniyan, S.; Jenekhe, S. A. All-Polymer Solar Cells with 3.3% Efficiency Based on Naphthalene Diimide-Selenophene Copolymer Acceptor. *J. Am. Chem. Soc.* **2013**, *135*, 14960−14963.
(24) Zhou, Y.; Kurosawa, T.; Ma, W.; Guo, Y.; Fang, L.; Vandewal, K.; Diao, Y.; Wang, C.; Yan, Q.; Reinspach, J.; Mei, J.; Appleton, A. L.; Koleilat, G. I.; Gao, Y.; Mannsfeld, S. C. B.; Salleo, A.; Ade, H.; Zhao, D.; Bao, Z. High Performance All-Polymer Solar Cell via Polymer Side-Chain Engineering. *Adv. Mater.* **2014**, *26*, 3767−3772.
(25) Zhou, E.; Cong, J.; Hashimoto, K.; Tajima, K. Control of Miscibility and Aggregation Via the Material Design and Coating Process for High-Performance Polymer Blend Solar Cells. *Adv. Mater.* **2013**, *25*, 6991−6996.
(26) Jiang, W.; Ye, L.; Li, X.; Xiao, C.; Tan, F.; Zhao, W.; Hou, J.; Wang, Z. Bay-linked Perylene Bisimides as Promising Non-Fullerene Acceptors for Organic Solar Cells. *Chem. Commun.* **2014**, *50*, 1024−1026.
(27) Zhang, X.; Lu, Z.; Ye, L.; Zhan, C.; Hou, J.; Zhang, S.; Jiang, B.; Zhao, Y.; Huang, J.; Zhang, S.; Liu, Y.; Shi, Q.; Liu, Y.; Yao, J. A Potential Perylene Diimide Dimer-Based Acceptor Material for Highly Efficient Solution-Processed Non-Fullerene Organic Solar Cells with 4.03% Efficiency. *Adv. Mater.* **2013**, *25*, 5791−5797.
(28) Pho, T. V.; Toma, F. M.; Chabinyc, M. L.; Wudl, F. Self-Assembling Decacyclene Triimides Prepared through a Regioselective Hextuple Friedel−Crafts Carbamylation. *Angew. Chem., Int. Ed.* **2013**, *52*, 1446−1451.
(29) Lin, Y.; Wang, Y.; Wang, J.; Hou, J.; Li, Y.; Zhu, D.; Zhan, X. A Star-Shaped Perylene Diimide Electron Acceptor for High-Performance Organic Solar Cells. *Adv. Mater.* **2014**, *26*, 5137−5142.
(30) Scharber, M. C.; Wuhlbacher, D.; Koppe, M.; Denk, P.; Waldauf, C.; Heeger, A. J.; Brabec, C. L. Design Rules for Donors in Bulk-Heterojunction Solar Cells - Towards 10% Energy-Conversion Efficiency. *Adv. Mater.* **2006**, *18*, 789−794.
(31) Cheng, Y.-J.; Yang, S.-H.; Hsu, C.-S. Synthesis of Conjugated Polymers for Organic Solar Cell Applications. *Chem. Rev.* **2009**, *109*, 5868−5923.
(32) Blouin, N.; Michaud, A.; Gendron, D.; Wakim, S.; Blair, E.; Neagu-Plesu, R.; Belletête, M.; Durocher, G.; Tao, Y.; Leclerc, M. Toward a Rational Design of Poly(2,7-Carbazole) Derivatives for Solar Cells. *J. Am. Chem. Soc.* **2007**, *130*, 732−742.
(33) Du, C.; Li, C. H.; Li, W. W.; Chen, X.; Bo, Z. S.; Veit, C.; Ma, Z. F.; Wuerfel, U.; Zhu, H. F.; Hu, W. P.; Zhang, F. L. 9-Alkylidene-9H-Fluorene-Containing Polymer for High-Efficiency Polymer Solar Cells. *Macromolecules* **2011**, *44*, 7617−7624.
(34) Wang, E.; Wang, L.; Lan, L.; Luo, C.; Zhuang, W.; Peng, J.; Cao, Y. High-Performance Polymer Heterojunction Solar Cells of a Polysilafluorene Derivative. *Appl. Phys. Lett.* **2008**, *92*, 033307.
(35) Wang, E.; Hou, L.; Wang, Z.; Hellström, S.; Zhang, F.; Inganäs, O.; Andersson, M. R. An Easily Synthesized Blue Polymer for High-Performance Polymer Solar Cells. *Adv. Mater.* **2010**, *22*, 5240−5244.
(36) Chen, H.-C.; Chen, Y.-H.; Liu, C.-C.; Chien, Y.-C.; Chou, S.-W.; Chou, P.-T. Prominent Short-Circuit Currents of Fluorinated Quinoxaline-Based Copolymer Solar Cells with A Power Conversion Efficiency of 8.0%. *Chem. Mater.* **2012**, *24*, 4766−4772.
(37) Chen, M.-H.; Hou, J.; Hong, Z.; Yang, G.; Sista, S.; Chen, L.-M.; Yang, Y. Efficient Polymer Solar Cells with Thin Active Layers Based on Alternating Polyfluorene Copolymer/Fullerene Bulk Heterojunctions. *Adv. Mater.* **2009**, *21*, 4238−4242.
(38) Hendriks, K. H.; Li, W.; Heintges, G. H. L.; van Pruissen, G. W. P.; Wienk, M. M.; Janssen, R. A. J. Homocoupling Defects in Diketopyrrolopyrrole-Based Copolymers and Their Effect on Photovoltaic Performance. *J. Am. Chem. Soc.* **2014**, *136*, 11128−11133.
(39) Li, W.; Roelofs, W. S. C.; Wienk, M. M.; Janssen, R. A. J. Enhancing the Photocurrent in Diketopyrrolopyrrole-Based Polymer Solar Cells via Energy Level Control. *J. Am. Chem. Soc.* **2012**, *134*, 13787−13795.
(40) Li, G.; Kang, C.; Li, C.; Lu, Z.; Zhang, J.; Gong, X.; Zhao, G.; Dong, H.; Hu, W.; Bo, Z. Planar Conjugated Polymers Containing 9,10-Disubstituted Phenanthrene Units for Efficient Polymer Solar Cells. *Macromol. Rapid Commun.* **2014**, *35*, 1142−1147.
(41) Wang, L.; Cai, D.; Zheng, Q.; Tang, C.; Chen, S.-C.; Yin, Z. Low Band Gap Polymers Incorporating a Dicarboxylic Imide-Derived Acceptor Moiety for Efficient Polymer Solar Cells. *ACS Macro Lett.* **2013**, *2*, 605−608.
(42) Wang, N.; Chen, Z.; Wei, W.; Jiang, Z. Fluorinated Benzothiadiazole-Based Conjugated Polymers for High-Performance Polymer Solar Cells without Any Processing Additives or Post-treatments. *J. Am. Chem. Soc.* **2013**, *135*, 17060−17068.
(43) Zhou, H. X.; Yang, L. Q.; Stuart, A. C.; Price, S. C.; Liu, S. B.; You, W. Enhanced Device Performance of Polymer Solar Cells by Planarization of Quinoxaline Derivative in a Low-Bandgap Polymer. *Angew. Chem., Int. Ed.* **2011**, *50*, 2995−2998.
(44) Qin, T.; Zajaczkowski, W.; Pisula, W.; Baumgarten, M.; Chen, M.; Gao, M.; Wilson, G.; Easton, C. D.; Müllen, K.; Watkins, S. E. Tailored Donor−Acceptor Polymers with an A−D1−A−D2 Structure: Controlling Intermolecular Interactions to Enable Enhanced Polymer Photovoltaic Devices. *J. Am. Chem. Soc.* **2014**, *136*, 6049−6055.
(45) Zhang, M.; Gu, Y.; Guo, X.; Liu, F.; Zhang, S.; Huo, L.; Russell, T. P.; Hou, J. Efficient Polymer Solar Cells Based on Benzothiadiazole and Alkylphenyl Substituted Benzodithiophene with a Power Conversion Efficiency over 8%. *Adv. Mater.* **2013**, *25*, 4944−4949.
(46) Zhou, E.; Cong, J.; Hashimoto, K.; Tajima, K. A Benzoselenadiazole-Based Low Band Gap Polymer: Synthesis and Photovoltaic Application. *Macromolecules* **2013**, *46*, 763−768.
(47) Huo, L.; Hou, J.; Zhang, S.; Chen, H.-Y.; Yang, Y. A Polybenzo[1,2-b:4,5-b′]dithiophene Derivative with Deep HOMO Level and Its Application in High-Performance Polymer Solar Cells. *Angew. Chem., Int. Ed.* **2010**, *49*, 1500−1503.

DOI: 10.1021/acsami.5b00026
ACS Appl. Mater. Interfaces 2015, 7, 10710−10717

(48) Han, L.; Bao, X.; Hu, T.; Du, Z.; Chen, W.; Zhu, D.; Liu, Q.; Sun, M.; Yang, R. Novel Donor−Acceptor Polymer Containing 4,7-Bis(thiophen-2-yl)benzo[c][1,2,5]thiadiazole for Polymer Solar Cells with Power Conversion Efficiency of 6.21%. *Macromol. Rapid Commun.* **2014**, *35*, 1153−1157.
(49) Zhou, P.; Zhang, Z.-G.; Li, Y.; Chen, X.; Qin, J. Thiophene-Fused Benzothiadiazole: A Strong Electron-Acceptor Unit to Build D−A Copolymer for Highly Efficient Polymer Solar Cells. *Chem. Mater.* **2014**, *26*, 3495−3501.
(50) Li, Y.; Chen, Y.; Liu, X.; Wang, Z.; Yang, X.; Tu, Y.; Zhu, X. Controlling Blend Film Morphology by Varying Alkyl Side Chain in Highly Coplanar Donor−Acceptor Copolymers for Photovoltaic Application. *Macromolecules* **2011**, *44*, 6370−6381.
(51) Wang, M.; Hu, X.; Liu, P.; Li, W.; Gong, X.; Huang, F.; Cao, Y. Donor−Acceptor Conjugated Polymer Based on Naphtho[1,2-c:5,6-c]bis[1,2,5]thiadiazole for High-Performance Polymer Solar Cells. *J. Am. Chem. Soc.* **2011**, *133*, 9638−9641.
(52) Li, G.; Kang, C.; Gong, X.; Zhang, J.; Li, C.; Chen, Y.; Dong, H.; Hu, W.; Li, F.; Bo, Z. 5-Alkyloxy-6-fluorobenzo[c][1,2,5]thiadiazole- and Silafluorene-Based D−A Alternating Conjugated Polymers: Synthesis and Application in Polymer Photovoltaic Cells. *Macromolecules* **2014**, *47*, 4645−4652.
(53) Huo, L. J.; Zhang, S. Q.; Guo, X.; Xu, F.; Li, Y. F.; Hou, J. H.Replacing Alkoxy Groups with Alkylthienyl Groups: A Feasible Approach To Improve the Properties of Photovoltaic Polymers. *Angew. Chem., Int. Ed.* **2011**, *50*, 9697−9702.
(54) Duan, R. M.; Ye, L.; Guo, X.; Huang, Y.; Wang, P.; Zhang, S. Q.; Zhang, J. P.; Huo, L. J.; Hou, J. H. Application of Two-Dimensional Conjugated Benzo[1,2-b:4,5-b]dithiophene in Quinoxaline-Based Photovoltaic Polymers. *Macromolecules* **2012**, *45*, 3032−3038.
(55) Min, J.; Zhang, Z.-G.; Zhang, S.; Li, Y. Conjugated Side-Chain-Isolated D-A Copolymers Based on Benzo[1,2-b:4,5-b′]dithiophene-alt-dithienylbenzotriazole: Synthesis and Photovoltaic Properties. *Chem. Mater.* **2012**, *24*, 3247−3254.
(56) Cho, N.; Song, K.; Lee, J. K.; Ko, J. Facile Synthesis of Fluorine-Substituted Benzothiadiazole-Based Organic Semiconductors and Their Use in Solution-Processed Small-Molecule Organic Solar Cells. *Chem.—Eur. J.* **2012**, *18*, 11433−11439.
(57) Li, G.; Lu, Z.; Li, C.; Bo, Z. The Side Chain Effect on Difluoro-substituted dibenzo[a,c]phenazine Based Conjugated Polymers as Donor Materials for High Efficiency Polymer Solar Cells. *Polym. Chem.* **2015**, *6*, 1613−1618.
(58) Franeker, J. J. V.; Turbiez, M.; Li, W.; Wienk, M. M.; Janssen, R. A. J. A Real-Time Study of The Benefits of Co-solvents in Polymer Solar Cell Processing. *Nat. Commun.* **2014**, *6*, 6229.
(59) Blom, P. W. M.; Mihailetchi, V. D.; Koster, L. J. A.; Markov, D. E. Device Physics of Polymer:Fullerene Bulk Heterojunction Solar Cells. *Adv. Mater.* **2007**, *19*, 1551−1566.

DOI: 10.1021/acsami.5b00026
ACS Appl. Mater. Interfaces 2015, 7, 10710−10717